JOURNAL OF MATERIALS SCIENCE 19 (1984) 167–182

The effect of edge stresses on the failure of (0°, 45°, 90°) CFRP laminates

P. T. CURTIS
Materials and Structures Department, Royal Aircraft Establishment, Farnborough, Hampshire, UK

Four (0°, 45°, 90°) CFRP laminates with different stacking sequences of plies were tested in tension, and the development of damage and failure processes was monitored by visual observation and acoustic emission. All four developed cracks across the 90° layers before final failure, the thicker 90° layers cracking at lower applied loads. Cracks also formed parallel to the plies at the edges of three of the four laminates and grew, with increasing load, towards the middle. A theoretical model was developed to calculate the normal stresses perpendicular to the plane of a laminate at its edges. Effects were included for the residual stresses caused by cooling from the moulding temperature and by moisture absorption by the epoxy resin. The theoretical predictions agreed well with the observed differences in longitudinal edge cracking and delamination tendency of the four laminates.

1. Introduction

The properties of unidirectional composites are highly anisotropic so that for applications employing sheet materials it is necessary to use laminates made from thin unidirectional plies with the fibres arranged in different directions in the various layers. In previous work it was shown [1–5] that laminate properties depend upon the thicknesses of the individual layers; for example, good laminate toughness and low notch sensitivity are usually obtained [1, 3] with thicker layers whereas thin layers can support greater loads without cracking [4, 5] when the fibre direction is transverse to (or at a large angle with respect to) that of the principle tensile stress. In addition, the properties of CFRP laminates depend upon the fibre orientations in neighbouring layers. This is because the Young's modulus, E_1, of each layer in the loading direction and the transverse modulus, E_2, and Poisson's ratio, ν, depend markedly upon the fibre direction; and, because the layers are stuck together, the differing in-plane transverse stresses, σ_y, in each layer [5] lead to out-of-plane normal stresses, σ_z, and shear stresses, τ_{yz} and τ_{xz}, at the edges of the laminate. The magnitudes of these edge stresses depend upon the stacking sequence of the layers and they vary through the laminate thickness, frequently having maxima at ply interfaces [6].

In the present work a simple theoretical model is used to predict the distribution of σ_z at the free edges of (0_3°, $\pm 45^\circ$, 90°) CFRP laminates with differing layer stacking sequences; and comparisons are made with the development of damage in tensile tests on the laminates.

2. Experimental details

Laminates were moulded from pre-impregnated warp sheets made from high-strength surface-treated carbon fibres in an epoxy resin with a moulded thickness of 0.125 mm. These sheets were stacked to give the following lay-ups:

$$A = [0_3^\circ, \pm 45^\circ, 90^\circ]_s$$

$$B = [0_3^\circ, 90^\circ, \pm 45^\circ]_s$$

$$C = [\pm 45^\circ, 0_3^\circ, 90^\circ]_s$$

$$D = [\pm 45^\circ, 90^\circ, 0_3^\circ]_s$$

An eight-ply unidirectional laminate and a four-ply $[\pm 45^\circ]_s$ laminate were also moulded for measuring the Young's modulus of 0°, 90° and ± 45° materials.

The laminates were cured in an autoclave at a temperature of 170° C for 1 h. The quality

of the moulded laminates was checked using ultrasonic c-scanning. The laminates were stored in a controlled environment (23° C and 65% RH) until they reached constant weight. This took a little over three months, in which time approximately 0.8% by weight of water was absorbed by the laminates. The fibre volume fraction, v_f, of the laminates was measured using an acid digestion technique.

Eight coupons of size 250 mm × 20 mm were cut from each laminate for tensile testing and end tags of etched aluminium alloy (L81) were bonded to the coupons using an epoxy resin adhesive cured at room temperature. Strain gauges, each 1 cm long, were bonded to every coupon along its axis for measuring the applied strain, and similar gauges were bonded across the widths of three coupons from each laminate for measuring Poisson's ratio. Foil strain gauges, each 1 mm long, were bonded to the edges (in the z-direction) of two coupons from each laminate to measure the edge strains.

Tensile tests were carried out on a screw driven machine at a constant crosshead speed of 0.02 mm sec^{-1}. Longitudinal stress–strain plots (σ_x against ϵ_x) were recorded for every coupon and the transverse ϵ_y and edge strains ϵ_z recorded for certain coupons. An acoustic emission monitoring system was used to obtain additional information on cumulative damage. A transducer was clamped to the coupons and the rate of acoustic emission monitored as a function of applied strain. Two specimens from each laminate were painted with a white emulsion paint so that surface damage could be readily observed by appearing black against a white background; the damage was recorded photographically. The edges of two coupons from each of the four laminates were polished and tests were interrupted at intervals of about 0.1% applied strain so that the edges could be examined with an optical microscope for signs of cracking. After failure, sections were cut, mounted, polished and examined using an optical microscope.

3. Results

3.1. Mechanical properties

The tensile stress–strain curves of the undirectional coupons tested in the fibre direction were nonlinear, Young's modulus increasing slightly with increasing strain. Failure involved a combination of fibre fracture, delamination between the plies and splitting parallel to the fibres within the plies. The 90° coupons had approximately linear stress–strain curves and failed by splitting parallel to the fibres at low strains. The stress–strain curves of the $[\pm 45°]_s$ coupons were nonlinear, the moduli falling rapidly with increasing applied strain.

TABLE I Mechanical properties of the 0°, 90° and $[\pm 45°]_s$ coupons

	0°	90°	$[\pm 45°]_s$
Failure stress (GPa)	1.79 ± 0.07	0.066	
Failure strain (%)	1.16 ± 0.04	0.7	–
Secant modulus at 0.1% strain (GPa)	140 ± 2	10.1	15.3
Secant modulus at failure (GPa)	155 ± 2	9.5	–
Poisson's ratio	0.34	–	0.45

Values for the 0°, 90° and $[\pm 45°]_s$ materials of the failure stresses and strains, secant moduli up to 0.1% applied strain and up to the failure strain and the measured Poisson's ratios are given in Table I. The failure stresses and strains of the $[\pm 45°]_s$ coupon are not listed, since final failure of these coupons was susceptible to surface flaws and occurred at widely variable applied strains. The fibre volume fractions of these laminates were approximately 65%. These values of modulus were used in the calculations in Section 4.

In all four (0, 45, 90) laminates, the slopes of the stress–strain curves decreased slightly with the development of longitudinal edge cracks. This is shown, for a coupon from laminate C, in Fig. 1, in which the slope of the stress–strain curve is also plotted. This reduction in tangent modulus was associated with edge cracking which was gradual and was not associated with any pronounced discontinuities in the traces. The plots of the transverse strain, ϵ_y, and edge strain, ϵ_z, did show discontinuities, but usually at higher strains than that at the onset of edge cracking. This was because the cracks were not necessarily first initiated in the strain gauge lengths, but once formed they usually grew quite rapidly in the x-direction, becoming continuous along the specimen length. Typical plots of ϵ_z against the applied strain ϵ_x are given in Fig. 2, showing discontinuities for laminates A, C and D. The

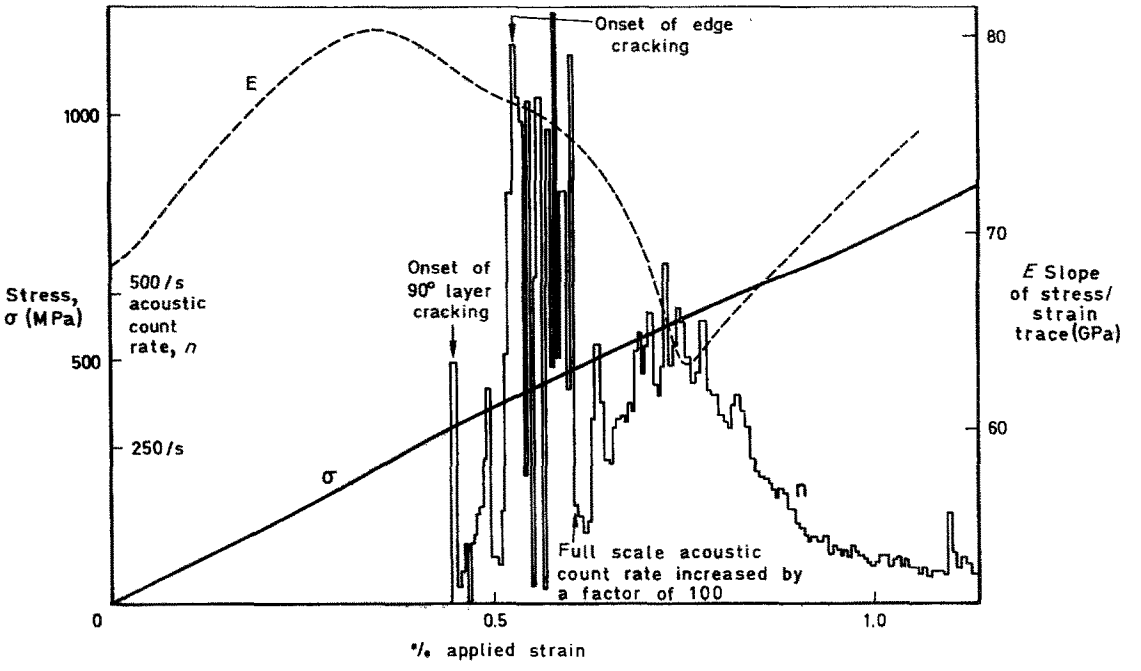

Figure 1 Acoustic count rate, applied stress and derivative of the applied stress as a function of applied strain for a typical coupon from laminate C.

apparent edge strain, ϵ_z, was negative for laminates A and B and positive for laminates C and D.

Values of the failure stresses and strains, secant moduli up to 0.25% applied strain and to failure, the major Poisson's ratios and the fibre volume fractions for the four laminates are given in Table II.

3.2. Observed failure modes

Observation of specimens with polished edges

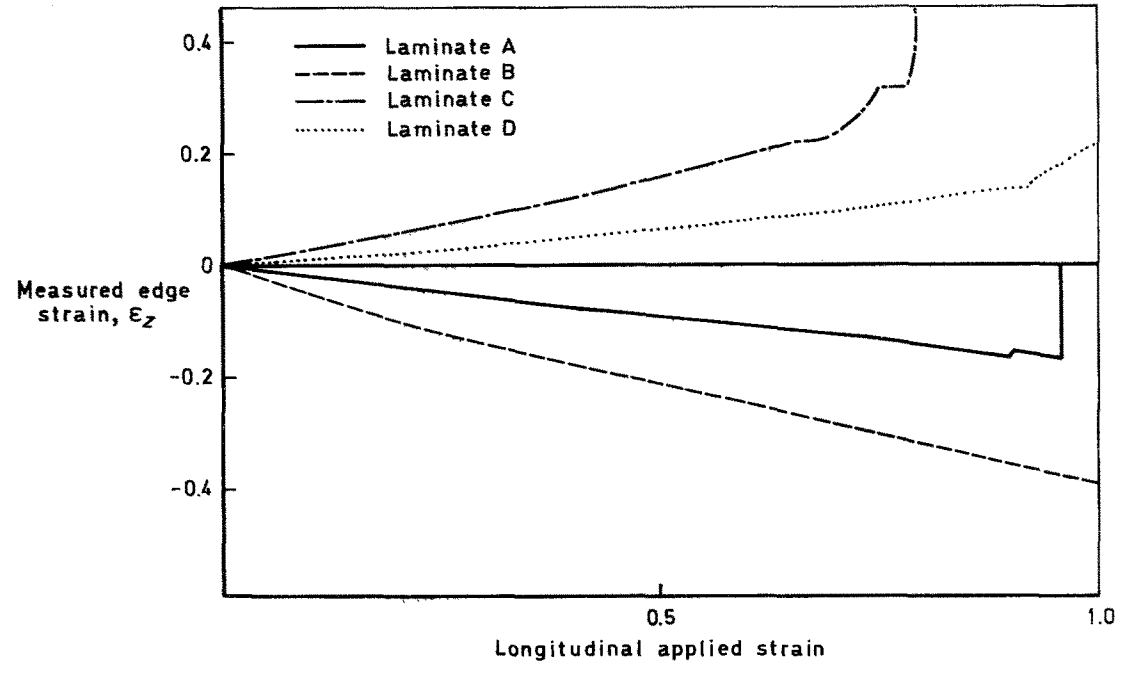

Figure 2 Measured z-direction strain at the edges of the four (0°, ± 45°, 90°) laminates tested as a function of applied strain ϵ_x.

TABLE II Mechanical properties of laminates A, B, C and D

	Laminate			
	A $[0^\circ_3, \pm 45^\circ, 90^\circ]_S$	B $[0^\circ_3, 90^\circ, \pm 45^\circ]_S$	C $[\pm 45^\circ, 0^\circ_3, 90^\circ]_S$	D $[\pm 45^\circ, 90^\circ, 0^\circ_3]_S$
Failure stress (MPa)	955 ± 55	960 ± 34	920 ± 65	990 ± 71
Failure strain (%)	1.10 ± 0.09	1.13 ± 0.05	1.14 ± 0.08	1.14 ± 0.09
Secant modulus at 0.25% strain (GPa)	84 ± 3	82 ± 3	83 ± 3	84 ± 3
Secant modulus at failure (GPa)	87 ± 3	83 ± 1	81 ± 2	87 ± 2
Poisson's ratio ν_{12}	0.32 ± 0.02	0.31 ± 0.02	0.32 ± 0.02	0.31 ± 0.02
Fibre volume fraction (%)	64	63	64	63

from all four laminates showed that the first damage to occur was transverse cracking of the 90° layers, at lower strains in the laminates with thick 90° layers, laminates A and C, than in the laminates with thin 90° layers, B and D (Table III). At small applied strains the cracks in the 90° layers stopped at the boundaries with adjacent layers. The cracks were usually confined to the resin or the fibre–resin interfaces, although on rare occasions they passed through fibres, see Fig. 3. Subsequent sectioning of the specimens showed that the cracks in the 90° layers ran across the full widths of the coupons. As the applied strain was increased, more cracks ran across the 90° layers until the mean spacing between cracks was similar to the thickness of the layer.

As the applied strain was further increased, delamination of the layer interfaces was observed at the ends of the cracks in the 90° layers. The delamination was more extensive at 90°/45° interfaces, which occurred in laminates A, B and D, and was usually in one direction along the interface, as shown by Fig. 4a. The extent of delamination increased with increasing applied strain and was followed by cracks in the adjacent 45° plies in the opposite direction to the layer delamination (Fig. 4b). When the cracks in the 45° ply reached the + 45°/− 45° ply interface they led to delamination for a short distance in the opposite direction to that at the 90°/45° interface (see Fig. 4c). This sequence of events was observed more frequently in laminates A and D than in laminate B. The cracks in the 45° plies were initiated at the coupon edges and did not extend in from the edges more than 1 to 2 mm. These short cracks in the 45° plies were not confined to the fibre direction, as suggested in Fig. 4c, but fractured some fibres, particularly when close to the 90°/45° interface. This feature is being investigated further [7, 8].

Laminates A, C and D developed cracks parallel

TABLE III Applied strains at the onset of 90° layer cracking and longitudinal edge cracking: All strains in %

	Laminate			
	A $[0^\circ_3, \pm 45^\circ, 90^\circ]_S$	B $[0^\circ_3, 90^\circ, \pm 45^\circ]_S$	C $[\pm 45^\circ, 0^\circ_3, 90^\circ]_S$	D $[\pm 45^\circ, 90^\circ, 0^\circ_3]_S$
First visible transverse crack in 90° layer	0.50	0.65	0.48	0.65
First acoustic emission	0.53 ± 0.05	0.62 ± 0.04	0.49 ± 0.03	0.70 ± 0.04
First visible longitudinal edge crack	0.80	none	0.62	1.05
First acoustic emission exceeding 10^3 counts per second	0.82 ± 0.06	none	0.62 ± 0.04	1.04 ± 0.07

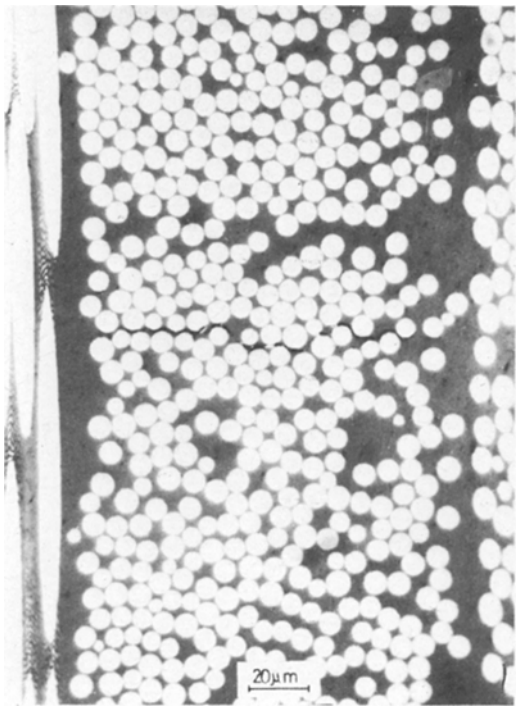

Figure 3 Typical crack across a single ply 90° layer (laminate D) before edge crack formation, × 312.

to the layers at their edges before failure but laminate B did not. This longitudinal edge cracking was detected by optical microscopy of coupons and confirmed by visual observation of the coupons painted white. Applied strains for the onset of edge cracking are listed in Table III. Fig. 5 shows a painted coupon from laminate C at four different stages of testing and shows the development of the longitudinal edge cracks. In Fig. 5a an edge crack has just been initiated; in Figs. 5b and c the opening displacement has increased with increasing applied strain; and Fig. 5d shows the failed coupon.

Inspection with the optical microscope showed a number of initiation sites for edge cracks such as the tips of cracks in the 90° layers, voids at ply interfaces and resin-rich regions within layers. In laminates A and C the edge cracks were propagated in the central 90° layer, either at the laminate mid-plane or along the adjacent layer interfaces, see Fig. 6, which is for a coupon from laminate A. In laminate D the edge cracks were initiated in the 90° layers, away from the mid-plane, and again tended to grow along the adjacent layer interfaces, as shown in Fig. 7. When edge cracks ran into transverse cracks in the layers, which had been initiated at lower applied strains, steps were formed as shown in Fig. 6. The opening displacement of the edge cracks became quite large in some cases, particularly in coupons from laminate C in which this was typically similar to the laminate thickness (Fig. 5).

All the coupons failed in tension across their widths. Fractured coupons from laminate A showed some longitudinal splitting (cracking within the layers in the fibre direction) of the outer 0° layers, but they failed mainly by fibre fracture in the transverse and 45° directions (see Fig. 8). Coupons from laminate B failed in a similar manner, except that the 0° layers showed much more evidence of failure in the transverse direction, this being interrupted by short splits in the longitudinal direction (see Fig. 9). Coupons from laminate C, which showed severe edge cracking, separated in half at failure, through the central 90° layer. Examination of this surface created by edge cracking revealed many transverse cracks in the central 90° layer. In addition, a narrow dark strip was observed in the centre of the width extending along the whole of the coupon length (see Fig. 10). This marks the limit of edge cracking just prior to coupon failure, when this narrow strip of intact resin fractured and the coupon separated into two halves. In these coupons, the 0° layers failed principally in the transverse direction, with occasional splitting parallel to the fibres as observed with coupons from laminate B. Some surface splitting in the outer 45° layers was also observed. Coupons from laminate D also showed 0° layer failures in the transverse directions.

3.3. Acoustic emission results

Fig. 1 gives the variation of acoustic emission count rate with applied strain for a coupon of laminate C – the laminate for which longitudinal edge cracking was the most severe. There was no acoustic emission during the initial elastic deformation of the coupon. The onset of emission was associated with the first observed transverse cracks in the 90° layer, and a large increase in count rate coincided with the occurrence of longitudinal edge cracking. With laminate C, there was a maximum in the count rate (note the change of scale by a factor of 100 in Fig. 1) at an applied strain of $0.8 \pm 0.04\%$ which coincided with a minimum value of tangent modulus. With coupons from laminates A and D the acoustic emission count rate was still increasing at failure. In lami-

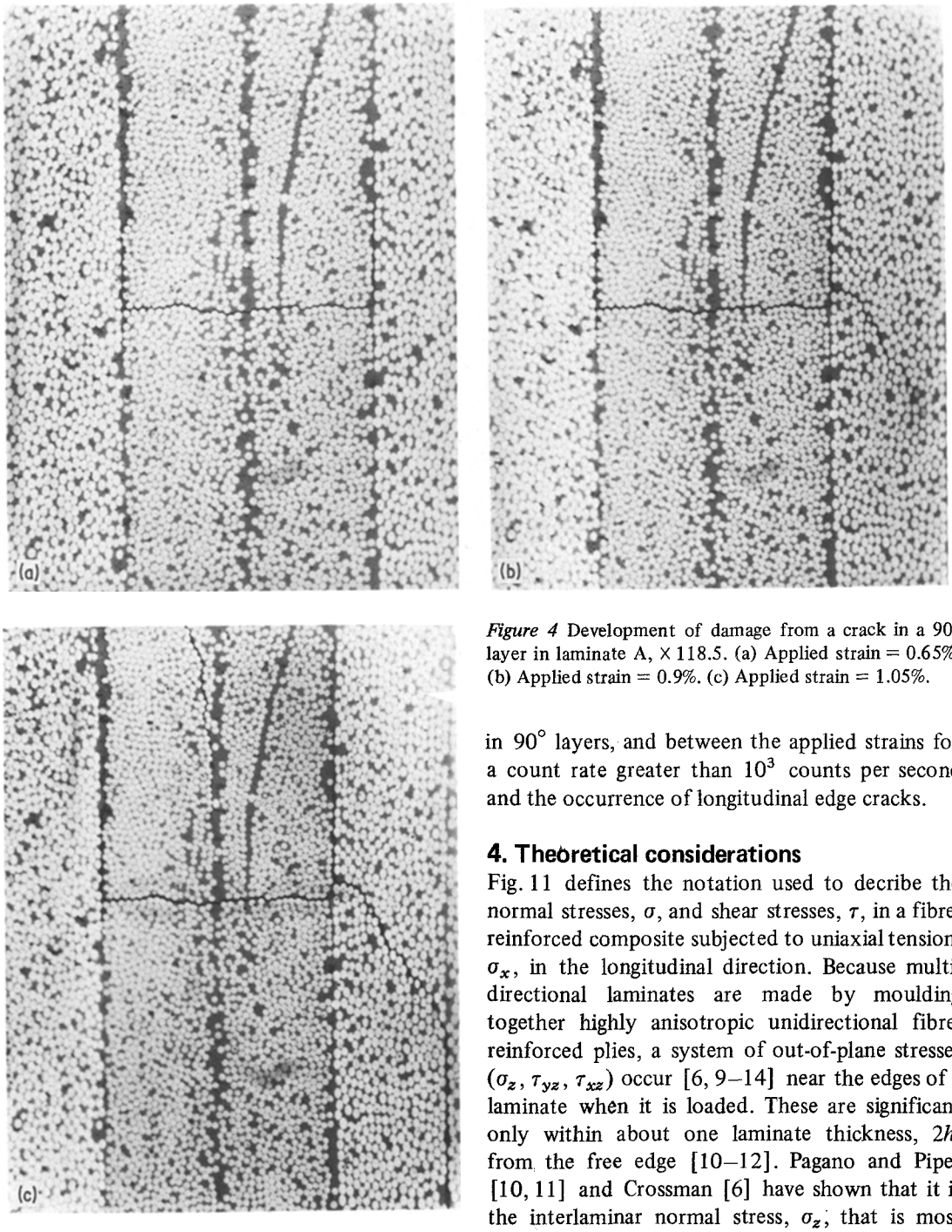

Figure 4 Development of damage from a crack in a 90° layer in laminate A, × 118.5. (a) Applied strain = 0.65%. (b) Applied strain = 0.9%. (c) Applied strain = 1.05%.

nate B, in which edge cracks were not observed, the acoustic emission was much smaller, never exceeding 10^3 counts per second at failure.

Table III shows that, for all four laminates investigated, there were good correlations between the applied strains for the onset of acoustic emission and the appearance of transverse cracks in 90° layers, and between the applied strains for a count rate greater than 10^3 counts per second and the occurrence of longitudinal edge cracks.

4. Theoretical considerations

Fig. 11 defines the notation used to decribe the normal stresses, σ, and shear stresses, τ, in a fibre-reinforced composite subjected to uniaxial tension, σ_x, in the longitudinal direction. Because multi-directional laminates are made by moulding together highly anisotropic unidirectional fibre-reinforced plies, a system of out-of-plane stresses (σ_z, τ_{yz}, τ_{xz}) occur [6, 9–14] near the edges of a laminate when it is loaded. These are significant only within about one laminate thickness, $2h$, from the free edge [10–12]. Pagano and Pipes [10, 11] and Crossman [6] have shown that it is the interlaminar normal stress, σ_z, that is most important in producing edge cracks under tensile loading. However, it has been argued [6] that it is primarily the interlaminar shear stresses that cause edge cracking in compression.

Numerical methods based on finite element and finite difference techniques have been used [6, 13, 14] to estimate laminate edge stresses; for example Pagano and Pipes [10, 11] give a curve

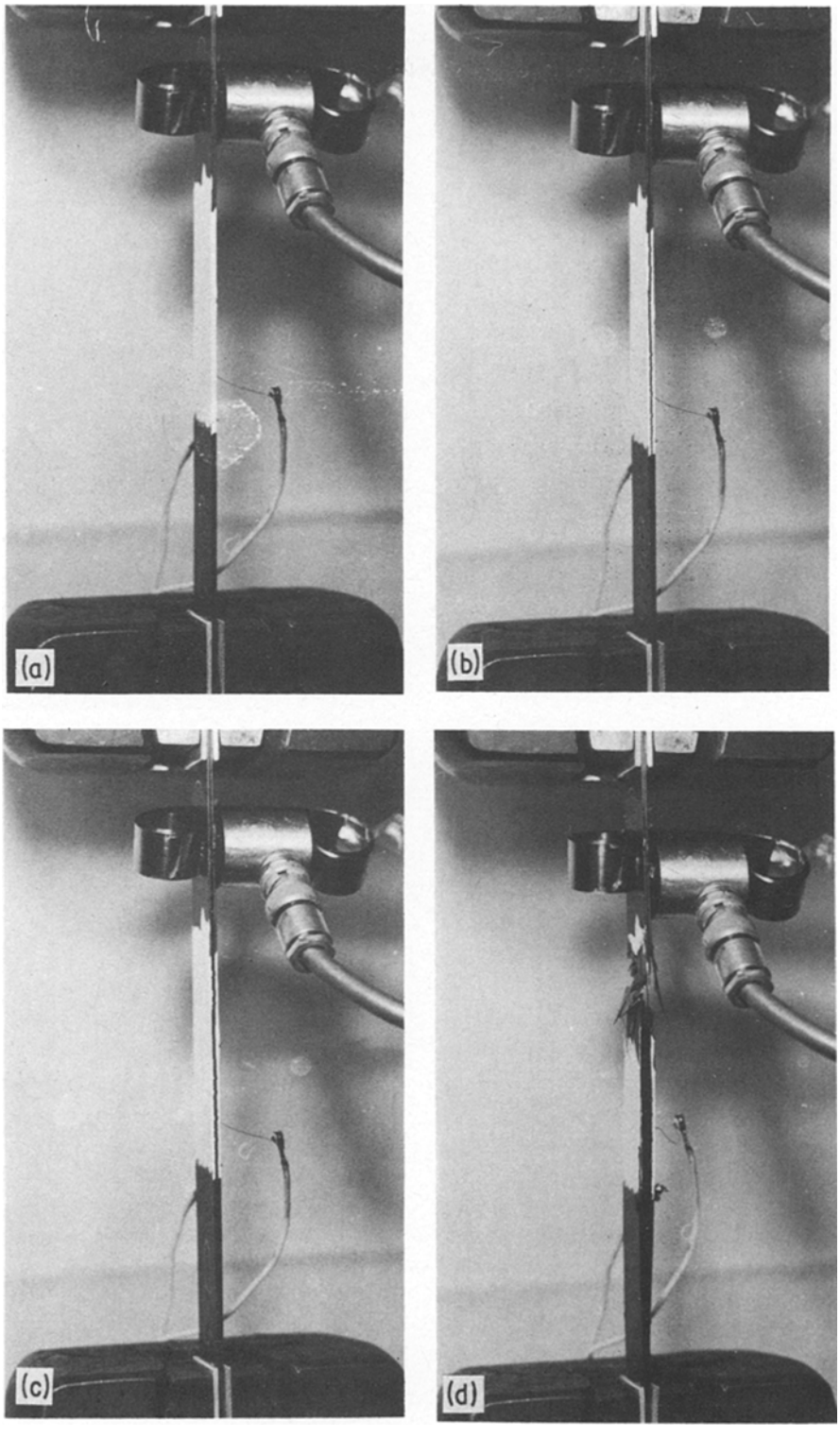

Figure 5 Development of edge cracking in a laminate C coupon (acoustic emission probe is clamped to testpiece), × 0.6. (a) Applied strain = 0.7%. (b) Applied strain = 0.85%. (c) Applied strain = 1.0%. (d) Applied strain = failure.

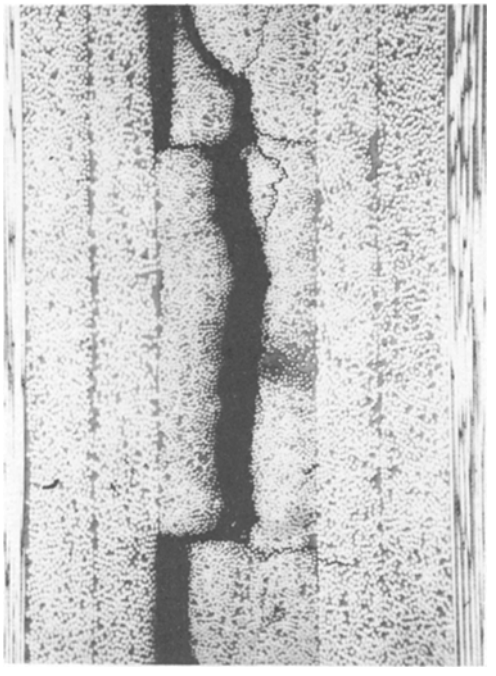

Figure 6 Typical edge cracking at failure in a laminate A coupon, × 55.2.

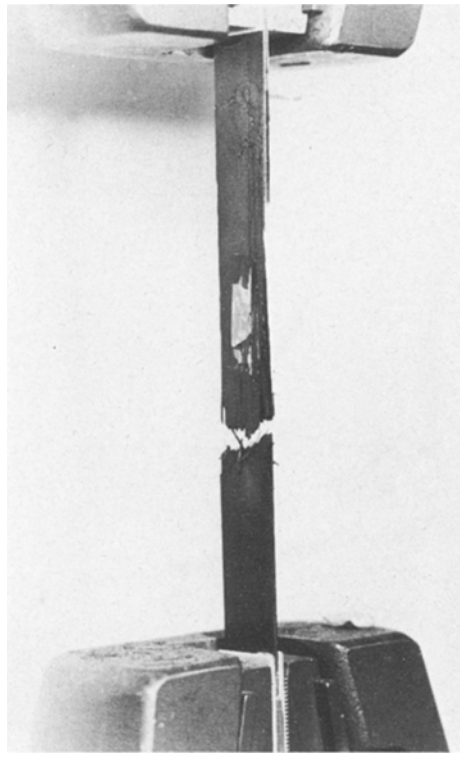

Figure 8 Failed coupon from laminate A, × 0.67.

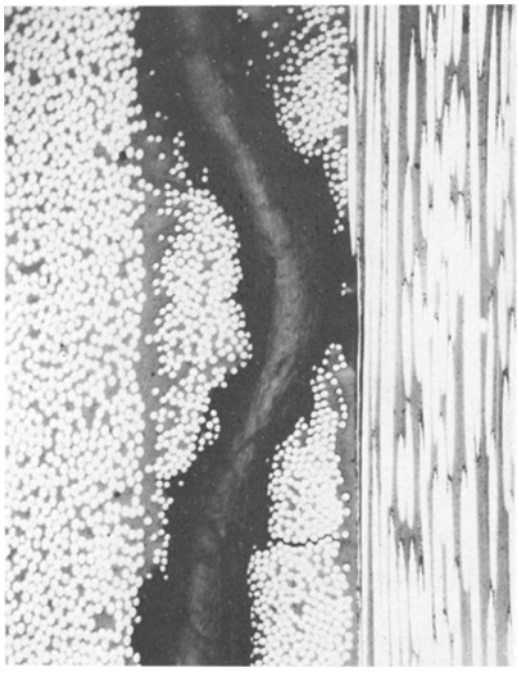

Figure 7 Typical edge cracking at failure in a laminate D coupon, × 92.

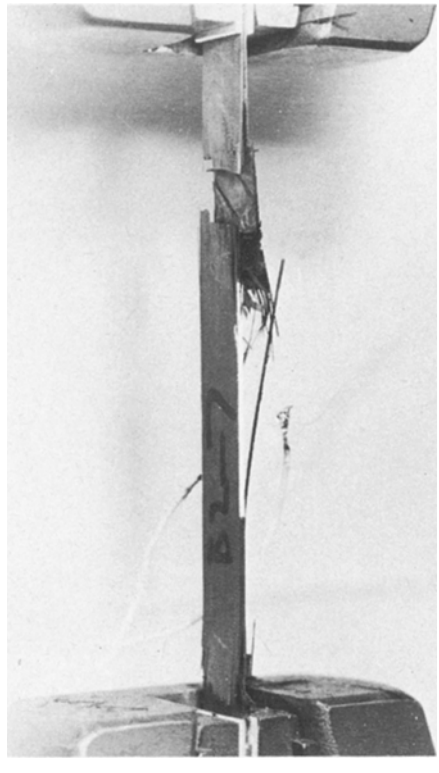

Figure 9 Failed coupon from laminate B, × 0.70.

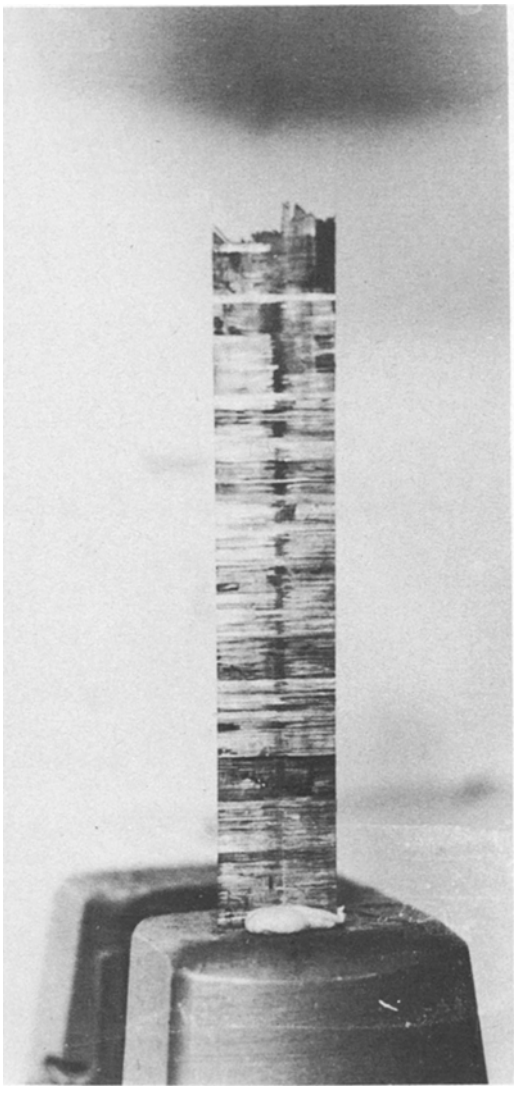

Figure 10 Part of failed coupon from laminate C, showing the extent of edge cracking in the central 90° layer, × 1.0.

for the variation of σ_z with y in the x–y plane of a laminate (see Fig. 12a); since numerical integration over this distribution is not a convenient method for investigating the effects of materials variables on edge stresses, simpler approaches based on approximate analytical expressions for $\sigma_z(y)$ have been used. Thus Harris and Orringer [9] assumed a distribution of the form given in Fig. 12b, and Pagano and Pipes [11] a distribution of the form given in Fig. 12c to estimate the normal stresses, σ_z, for $(\pm\theta_1, \pm\theta_2)$ laminates. In both cases the moment resulting from the distribution of positive σ_z must be equal and of opposite sign to that from negative σ_z, and the maximum value of σ_z occurs at the free edge of the laminates. The variation of σ_z at the free edge with distance Z through the laminate thickness was determined by relating σ_z with the transverse stresses, σ_y, calculated from laminated plate theory [15]. A similar approach is used in this paper for $(0°, \pm 45°, 90°)$ laminates, but effects are also included in the analysis for residual stresses caused by cooling from the moulding temperature and by moisture absorption by the epoxy resin [16].

Consider a laminate with a balanced symmetric lay-up containing layers with fibres at 0°, ± 45° and 90° to the x-axis (see Fig. 13); the total layer thickness of each type of layer is $2h_1$, $2h_2$ and $2h_3$, respectively, and the thickness of the total laminate is $2h$. When the laminate is subjected to a tensile load in the x-direction, the transverse stresses σ_y^0, σ_y^{45} and σ_y^{90} in the 0°, ± 45° and 90° layers, respectively, are related to the laminate strains ϵ_x and ϵ_y by:

$$\sigma_y^0 = \epsilon_x \bar{Q}_{xy}^0 + \epsilon_y \bar{Q}_{yy}^0 \quad (1)$$

$$\sigma_y^{45} = \epsilon_x \bar{Q}_{xy}^{45} + \epsilon_y \bar{Q}_{yy}^{45} \quad (2)$$

$$\sigma_y^{90} = \epsilon_y \bar{Q}_{xy}^{90} + \epsilon_y \bar{Q}_{yy}^{90} \quad (3)$$

in which the reduced stiffnesses, $\bar{Q}_{xy}$ and $\bar{Q}_{yy}$, of the layers depend upon the elastic constants of a unidirectional fibre-reinforced composite – Young's moduli, E_1 and E_2, parallel and perpendicular to the fibres, the in-plane shear modulus, G_{12}, and the in-plane Poisson's ratios, ν_{12} and ν_{21}, and upon the angle θ between the fibres in the layer and the x-direction. Thus,

$$\bar{Q}_{xy} = (Q_{xx} + Q_{yy} - 4Q_{zz}) \sin^2\theta \cos^2\theta + Q_{zz}(\sin^4\theta + \cos^4\theta) \quad (4)$$

$$\bar{Q}_{yy} = Q_{xx} \sin^4\theta + Q_{yy} \cos^4\theta + 2(Q_{xy} + 2Q_{zz}) \sin^2\theta \cos^2\theta \quad (5)$$

$$Q_{xx} = E_1/(1 - \nu_{12}\nu_{21}) \quad (6)$$

$$Q_{yy} = E_2/(1 - \nu_{12}\nu_{21}) \quad (7)$$

$$Q_{xy} = \nu_{12}E_2/(1 - \nu_{12}\nu_{21}) \quad (8)$$

$$Q_{zz} = G_{12}. \quad (9)$$

This use of laminated plate theory [15] assumes that the material behaviour is linear elastic, but this may not always be justified with fibre-reinforced composites. A better approximation may be obtained by using measured elastic constants at a specific applied strain (secant moduli,

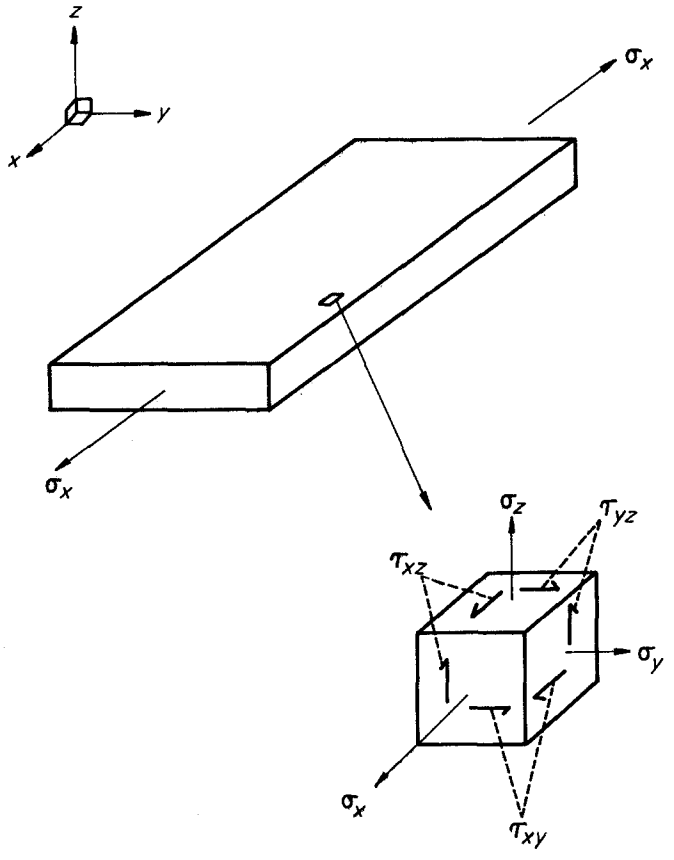

Figure 11 Details of the stresses developed in a fibre composite laminate subjected to a uniaxial stress, σ_x.

etc), for each layer in the particular laminate being considered. The balance of forces in the y-direction gives:

$$\sigma_y^0 h_1 + \sigma_y^{45} h_2 + \sigma_y^{90} h_3 = 0. \tag{10}$$

Equations 1, 2, 3 and 10 may then be solved to give the σ_y in terms of the strain ϵ_x due to the applied tensile load

$$\sigma_y^0 = \frac{-\epsilon_x [h_2(\bar{Q}_{xy}^{45}\bar{Q}_{yy}^0 - \bar{Q}_{yy}^{45}\bar{Q}_{xy}^0) + h_3(\bar{Q}_{xy}^{90}\bar{Q}_{yy}^0 - \bar{Q}_{yy}^{90}\bar{Q}_{xy}^0)]}{\bar{Q}_{yy}^0 h_1 + \bar{Q}_{yy}^{45} h_2 + \bar{Q}_{yy}^{90} h_3} \tag{11}$$

$$\sigma_y^{45} = \frac{-\epsilon_x [h_1(\bar{Q}_{xy}^0\bar{Q}_{yy}^{45} - \bar{Q}_{xy}^{45}\bar{Q}_{yy}^0) + h_3(\bar{Q}_{xy}^{90}\bar{Q}_{yy}^{45} - \bar{Q}_{yy}^{90}\bar{Q}_{xy}^{45})]}{\bar{Q}_{yy}^0 h_1 + \bar{Q}_{yy}^{45} h_2 + \bar{Q}_{yy}^{90} h_3} \tag{12}$$

$$\sigma^{90} = \frac{-\epsilon_x [h_2(\bar{Q}_{xy}^0\bar{Q}_{yy}^{90} - \bar{Q}_{yy}^0\bar{Q}_{xy}^{90}) + h_2(\bar{Q}_{xy}^{45}\bar{Q}_{yy}^{90} - \bar{Q}_{yy}^{45}\bar{Q}_{xy}^{90})]}{\bar{Q}_{yy}^0 h_1 + \bar{Q}_{yy}^{45} h_2 + \bar{Q}_{yy}^{90} h_3}. \tag{13}$$

To calculate the distribution of σ_z at the edge of a laminate, consider any plane z = constant and let p equal any distance in the z-direction from this plane. The moment $m(z)$ due to σ_y is given by integrating $p\sigma_y(p)\mathrm{d}p$ over the laminate thickness from the plane of interest to the laminate surface, i.e.

$$m(z) = \int_0^z p\sigma_y(p)\mathrm{d}p \tag{14}$$

where z is the position of the laminate surface relative to this plane. To proceed further it is necessary to assume a distribution of $\sigma_z(y)$. In this paper the distribution used by Pagano and Pipes [11], of the form given in Fig. 12c, is used where σ_z is a maximum at the laminate edge. In terms of this $\sigma_z(\max)$ the moment generated by this distribution is

$$m(z) = \frac{14h^2\sigma_z(\max)}{45}. \tag{15}$$

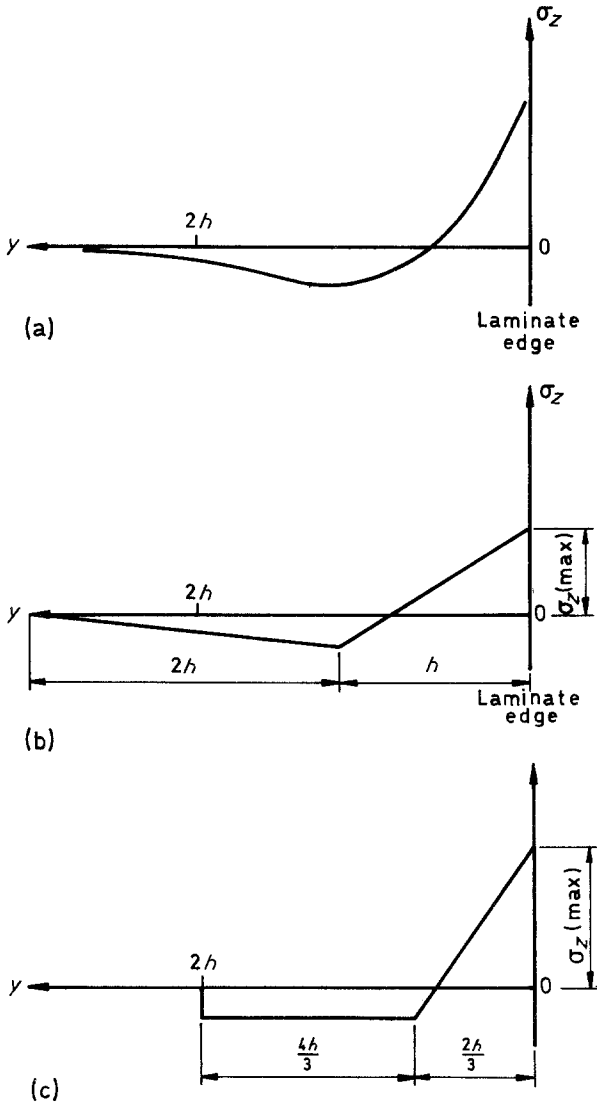

Figure 12 Distribution of normal stress σ_z against y. (a) Typical finite element solution. (b) Harris and Orringer distribution. (c) Pagano and Pipes distribution.

By equating the moments given in Equations 14 and 15, substituting for the stresses in the y-direction from Equations 11, 12 and 13 and including residual stresses, the value of the normal stress σ_z(max) at the laminate edge can be calculated for each x–y plane to give the distribution of σ_y through the laminate thickness.

For the four laminates tested in this work, the variation of normal edge stress σ_z was calculated for an applied strain of 1.14% since they all failed, see Section 3.1, at about this value. The results are given in Fig. 14. It can be seen that σ_z is large at the mid-plane of laminates A and C where the fibre orientation is at 90° to the applied load, much smaller in the 90° layers of laminate D and least in laminate B.

5. Discussion

5.1. Failure modes

Although the damage and failure processes in all four (0_3°, $\pm 45^\circ$, 90°) laminates tested had a number of common features, there were significant differences associated with particular ply stacking sequences – differences which can be important for the selection of layer thicknesses and orientations to enable fibre-reinforced laminates to support their design loads.

Thus in all cases the initial damage due to tensile loading in the x-direction was transverse cracking in the y–z plane parallel to the fibres in the 90° layers. However, the applied strain for the onset of this cracking was less for laminates A and C in which the 90° layers were twice as thick than

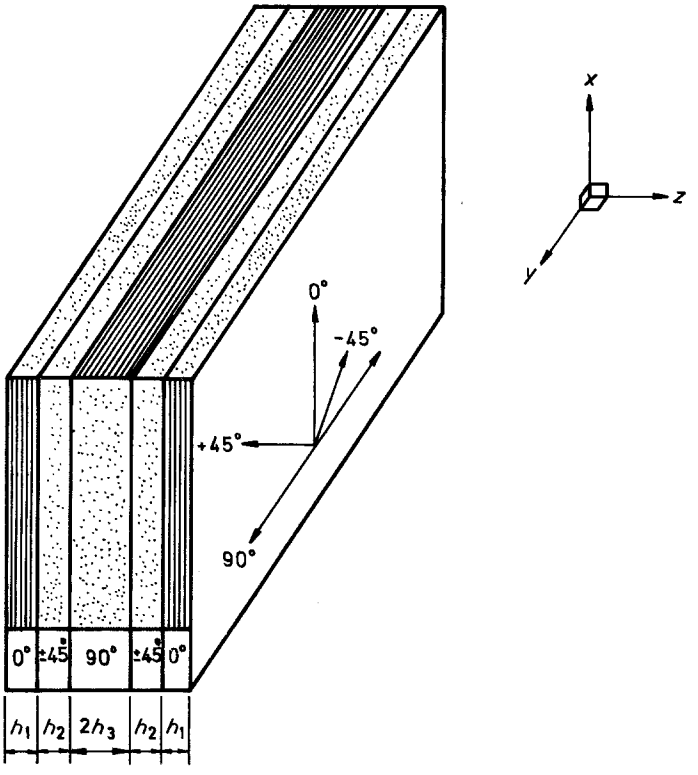

Figure 13 Typical lay-up of a $[0°, \pm 45°, 90°]_s$ laminate.

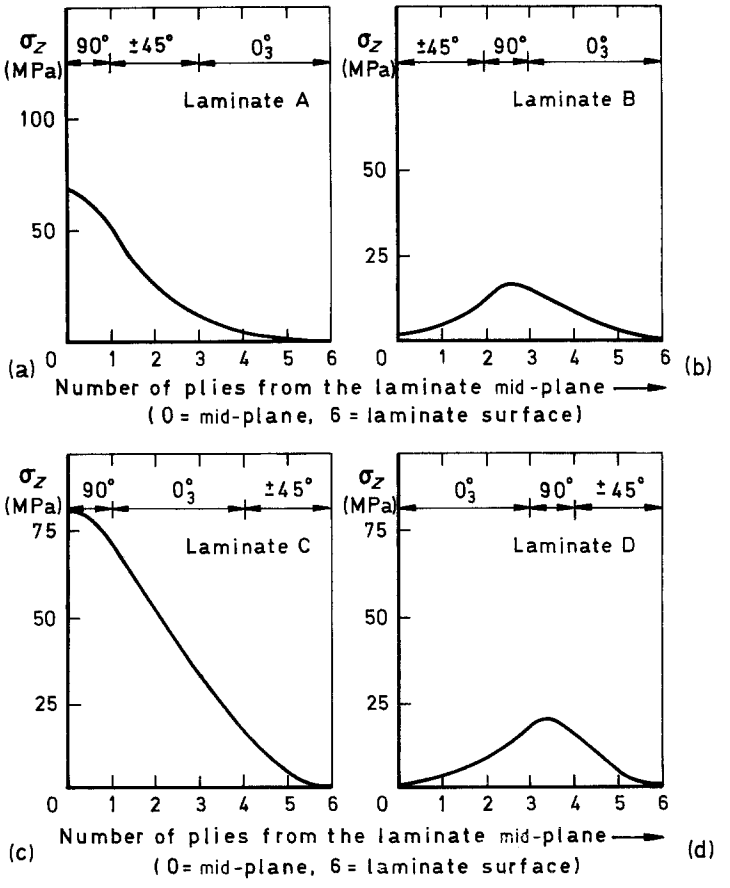

Figure 14 Theoretical variation of interlaminar normal stress, σ_z, at the edge of the laminates as a function of distance from the laminate midplane in the z-direction. (a) Laminate A – $[0^\circ_3, \pm 45°, 90°]_s$. (b) Laminate B – $[0^\circ_3, 90°, \pm 45°]_s$. (c) Laminate C – $[\pm 45°, 0^\circ_3, 90°]_s$. (d) Laminate D – $[\pm 45°, 90°, 0^\circ_3]$.

for laminates B and D. Similar cracking was observed in previous work with 0°, 90° laminates [4, 5], in which the increased cracking strain in thin 90° layers was attributed to constraints on crack initiation due to adjacent layers.

As the applied strain was increased, delamination was initiated at the ends of the 90° layer cracks, more readily at 90°/45° interfaces than at 0°/90° interfaces, probably due to the higher interlaminar shear stresses at the 90°/45° interfaces [6, 13, 14]. This delamination and subsequent cracking of the 45° plies was more common in laminates A and D than in laminate B. This suggests that the normal stress, σ_z, at the laminate edges, which (see Section 4), was greater in laminates A and D than in laminate B, was also contributing to the delamination at the 90°/45° interfaces. However, the observed delamination at the $+45°/-45°$ interface in laminate B shows that large interlaminar shear stresses were generated at this interface, and these were mainly responsible for delamination, since the normal stresses at the edge of this laminate were small. Thus it may be concluded that the small amounts of delamination observed at the ends of the 90° layer cracks were determined by the magnitudes of both the normal and shear stresses and that if either or both were sufficiently large, then delamination occurred readily. The extent of delamination could be increased under fatigue loading, as has been observed for CFRP crossply laminates [4]. At larger applied strains, cracks were initiated in the 45° plies adjacent to the 90° layers at the ends of the cracks in the 90° layers. When observed in the x–z plane, these cracks were at 45° to the cracks in the 90° layer; this was probably due to the complex stress fields at the ends of the 90° layer cracks, a result of load shedding of the 90° layer on cracking and the constraint exerted, on one side in the fibre direction by the stiff 90° layers and on the other side by the −45° ply. This would also explain the broken fibres observed in the x–y sections in the 45° plies.

At greater applied strains, longitudinal edge cracking occurred in laminates A and D and particularly in laminate C. Although these cracks were initiated at local stress concentrators such as voids, resin-rich regions, ply interfaces, or transverse cracks in the 90° layers, they were quite distinct from the small levels of delamination observed at lower strains at the ends of the 90° layer cracks: they had large opening displacements in the z-direction, they extended the whole gauge length of the coupons under load and were not confined to layer interfaces, and they were associated (see Section 3.3) with large outbursts, greater than 10^3 counts per second, of acoustic emission. The effect of ply stacking sequence on the susceptibility of a laminate to edge cracking is discussed in Section 5.2.

Although there were differing amounts of the above forms of damage in the four laminates, final tensile failure involves fracture of the 0° fibres so that the tensile strengths (see Section 5.3) were similar.

5.2. Comparison between theory and experiment

In general there was a good correlation between the theoretical predictions (Fig. 14) of the distribution of normal stress, σ_z, at the edges of laminates and the observed susceptibilities to longitudinal edge cracking under tensile loading, see Section 3.2, and Table IV.

Thus the order of edge cracking in the laminates was that given by the maximum predicted values for out-of-plane normal edge stress, σ_z. However, the initiation of edge cracks in the various laminates did not occur at the same value of σ_z. This was partly due to the approximations involved in the model, in particular the secant modulus of the $[\pm 45°]_s$ material. In addition, the interlaminar shear stresses, τ_{xz} and τ_{yz} have some

TABLE IV

	Calculated maximum value of σ_z (MPa)	Estimated σ_z at the onset of edge cracking (MPa)	Applied strain for onset of edge cracking (%)
Laminate C $[\pm 45°, 0°_3, 90°]_s$	82	65	0.62
Laminate A $[0°_3, \pm 45°, 90°]_s$	68	56	0.80
Laminate D $[\pm 45°, 90°, 0°_3]_s$	20	19	1.05
Laminate B $[0°_3, 90°, \pm 45°]_s$	16	–	none observed

TABLE V Comparison of theoretical and experimental edge strains (ϵ_z) at an applied strain of 0.5% for the four 0°, 45°, 90° laminates, averaged over the central eight plies of the laminates. All strains in %

	Edge strain			
	Laminate A $[0_3^\circ, \pm 45^\circ, 90^\circ]_S$	Laminate B $[0_3^\circ, 90^\circ, \pm 45^\circ]_S$	Laminate C $[\pm 45^\circ, 0_3^\circ, 90^\circ]_S$	Laminate D $[\pm 45^\circ, 90^\circ, 0_3^\circ]_S$
Corresponding to theoretical σ_z	+ 0.196	+ 0.089	+ 0.421	+ 0.133
From residual streses alone	+ 0.114	+ 0.059	+ 0.134	+ 0.020
From Poisson shrinkage alone	− 0.17	− 0.17	− 0.17	− 0.17
Total calculated ϵ_z	− 0.088	− 0.140	+ 0.117	− 0.057
Measured ϵ_z	− 0.097	− 0.207	+ 0.140	+ 0.058

Note: (a) Positive strains are tensile, negative strains compressive.
(b) The strains causing the edge cracking are those corresponding to σ_z.

influence. These are known to be especially large at layer interfaces bounded by one or more 45° plies [6, 13, 14], such as the 90°/45° interfaces in laminates A and D. This appears to be supported by experimental observations of edge cracking in laminates A and D. The theory predicted the lowest values of σ_z in laminates B and hence a low probability of edge cracking, and this was confirmed by the experiments. The good overall agreement between the values of σ_z calculated by the theory and the incidences of edge cracking in these laminates, shows that the magnitude of σ_z is the main factor determining whether edge cracks were formed in laminates in tension and that the interlaminar shear stress contributes to a lesser extent.

The edge strains measured experimentally were averaged of the z-direction displacements of the middle eight plies of the laminates. To compare these measured values with theoretical estimates one needs to calculate:

1. the strain ϵ_z corresponding to σ_z calculated in the theoretical Section 4 (assuming E_2 to be equal to E_3);
2. the strain ϵ_z resulting from the residual curing stresses, σ_y, since these were present in the laminates when the strain gauges were attached; and
3. the strain ϵ_z caused by the contraction in the z-direction due to Poisson's ratio.

The calculated and measured values of ϵ_z for applied strains of 0.5% are compared to Table V, and it can be seen that the agreement is quite good.

Other general conclusions concerning the magnitude of σ_z stresses developed in any laminates may be made from the theory. If the 90° layers are near or at the surface of laminates loaded in tension, the σ_z stresses developed will be compressive and of high magnitude. Under applied compressive loads, the reverse will occur and large tensile σ_z stresses will be generated. Other workers [6] have implied that the interlaminar shear stresses developed at the laminate edge may be more important than the normal stresses in determining whether edge cracking occurs under compressive applied loads, but a large tensile normal stress is indicative of susceptibility to edge cracking. If the 90° layers are near the mid-planes of laminates, the σ_z stresses produced are usually large and positive for applied tensile loads. Hence if large tensile normal stresses, σ_z, are important in determining whether laminates develop edge cracks under applied compressive loads, as was the case for applied tensile loads, then the selection of stacking sequences of laminates subjected to both tensile and compressive loads should be to minimize the absolute value of σ_z, rather than make it negative. Small values of σ_z are generated when the layers in which there are large transverse stresses σ_y are at or near the mid-planes of laminates, so that the moments they generate are small. Thus ± 45° layers should be placed near the laminate mid-planes, and, of the four laminates tested experimentally, only laminates B, the laminate with a central ± 45° layer, did not develop edge cracks. The two untested laminates of the six possible combinations of ± 45°, 0_3° and 90° layers would have 90° layers on their surfaces and would not be suitable for practical applications. They would not have cracked at their edges under tensile

loading, but under compressive loading. They would have relatively large tensile edge stresses and be susceptible to edge cracking.

In bending, the situation is more complex and layer stacking should take account of the edge stresses produced by the distribution of x-direction stresses through the laminate thickness.

Application of alternating loads would probably result in further growth of edge cracks and this could lead to the loss of the structural integrity of the laminates and a reduction in their fatigue lives.

In this work, moulding stresses have been allowed for by calculating strains for one specific environment, 65% RH and 23° C; but in a drier environment the residual strains in the laminates would be greater [16], and this would result in larger edge stresses and edge cracking at lower applied strains. The reverse would happen in more humid environments and edge cracking would not occur until greater applied strains than indicated in Section 4.

Thus, to minimize the probability of longitudinal edge cracking, either the layers with high Poisson's ratios, such as the ± 45° layers, should be positioned near the laminate mid-plane and surface and central 90° layers avoided, or the layers should be thin and well dispersed through the laminate thickness. However, although laminates with thin layers are less susceptible to edge cracking they are also less tough than laminates with thick layers [1, 3], thus the laminate design must be optimized according to the conditions of service.

5.3. Mechanical properties

Despite the observation that three of the four 0°, 45°, 90° laminates tested developed cracks at their edges before failure, these laminates were no weaker than the fourth laminate. The only observable difference between the mechanical properties of these laminates was that the failure stresses and strains in laminate B, which did not develop edge cracks, showed much less scatter than the other three laminates. This suggests that the presence of edge cracks did not reduce the strength of the load-bearing 0° layers. The stacking sequence of the layers had no significant effect on the Young's modulus and the Poisson's ratios of the laminates. However, the final fracture path was influenced by damage in the adjacent layers, in particular adjacent 90° layers which were severely cracked caused the 0° layers to fail in straight lines across the coupon widths.

6. Summary and conclusions

In summary, transverse cracks developed in the 90° layers of all four (0_3°, ± 45°, 90°) laminates at small applied strains, the thicker 90° layers cracking at the lowest applied strains. This was followed by delamination at the interface between the layers at the ends of these transverse cracks, particularly between ± 45° and 90° layers. Cracks also developed in the ± 45° layers near the tips of those in the 90° layers and grew with increasing applied strain until the + 45°/− 45° interface was reached, causing some delamination. The static strength of the laminates was not affected by this damage, but it could lead to environmental degradation and to loss of strength and stiffness in fatigue loading. At larger applied strains this initial damage was overtaken by longitudinal edge cracking, observed in three of the four laminates tested. A good correlation was obtained between small levels of acoustic emission and the initial damage and between large levels of acoustic emission and edge cracking. The strengths of the laminates did not depend upon lay-up, but there was slightly more scatter in the values for the three laminates that developed edge cracks.

From the result it was concluded that:

1. a simple theoretical model based on laminated plate theory but including the residual stresses caused by cooling from the moulding temperature and by moisture absorption by the epoxy resin, can be used to predict the distribution of the normal stresses, σ_z, at the edge of multidirectional CFRP laminates;

2. there was good agreement between the predictions of σ_z for (0_3°, ± 45°, 90°) laminates of various layer stacking sequences, and their observed susceptibilities to deleterious longitudinal edge cracking;

3. it was shown that edge cracking could be eliminated either by minimizing σ_z by positioning ± 45° layers near the laminate mid-plane and avoiding surface or central 90° layers or by using thin layers well-dispersed throughout the laminate thickness.

Acknowledgement

This paper is published by kind permission of the Royal Aircraft Establishment.

References

1. SARAH M. BISHOP and K. S. MCLAUGHLIN, RAE Technical Report 79051 (1979).
2. R. W. WALTER, R. W. JOHNSON, R. R. JUNE and J. E. MCCARTY, ASTM STP 636, edited by K. L. Reifsnider and K. N. Lauraitis (American Society for Testing and Materials, Philadelphia, 1977) p. 228.
3. P. T. CURTIS and G. DOREY, RAE Technical Report 79183 (1979).
4. P. T. CURTIS, M. G. BADER and J. E. BAILEY, MOD Research Agreement Report, Surrey University, Guildford (1978).
5. J. E. BAILEY, P. T. CURTIS and A. PARVIZI, *Proc. R. Soc. Lond.* **A366** (1979) 599.
6. F. W. CROSSMAN, Lockheed Palo Alto Research Laboratory Report, Palo Alto, California, USA (1978).
7. P. T. CURTIS, RAE Technical Report 80054 (1980).
8. *Idem, ibid.* 83011 (1983).
9. A. HARRIS and O. ORRINGER, *J. Comp. Mater.* **12** (1978) 285.
10. N. J. PAGANO and R. B. PIPES, *ibid.* **5** (1971) 50.
11. *Idem, Int. J. Mech. Sci.* **15** (1973) 679.
12. N. J. PAGANO, *J. Comp. Mater.* 8 (1974) 65.
13. A. S. D. WANG and F. W. CROSSMAN, *ibid.* **11** (1977) 92.
14. *Idem, ibid.* **12** (1978) 76.
15. J. E. ASHTON, J. C. HALPIN and P. H. PETIT, "Primer on composite materials: analysis", Technomic, Stamford (1969) Ch. 3.
16. P. T. CURTIS, RAE Technical Report 80045 (1980).

Received 27 January
and accepted 9 May 1983